Received: 29 May 2020 | Revised: 24 December 2020 | Accepted: 17 February 2021

DOI: 10.1111/ejn.15152

SPECIAL ISSUE ARTICLE

EJN European Journal of Neuroscience FENS WILEY

Single-trial regression of spatial exploration behavior indicates posterior EEG alpha modulation to reflect egocentric coding

Lukas Gehrke[1] | **Klaus Gramann**[1,2,3]

[1]Biopsychology and Neuroergonomics, Institute of Psychology and Ergonomics, Berlin, Germany

[2]Center for Advanced Neurological Engineering, University of California San Diego, San Diego, CA, USA

[3]School of Computer Science, University of Technology Sydney, Sydney, NSW, Australia

Correspondence
Lukas Gehrke, Biopsychology and Neuroergonomics, Institute of Psychology and Ergonomics, Fasanenstr. 1, KWT-1, 10623 Berlin, Germany.
Email: lukas.gehrke@tu-berlin.de

Funding information
Bundesministerium für Bildung und Forschung, Grant/Award Number: 01GQ1511

Abstract

Learning to navigate uncharted terrain is a key cognitive ability that emerges as a deeply embodied process, with eye movements and locomotion proving most useful to sample the environment. We studied healthy human participants during active spatial learning of room-scale virtual reality (VR) mazes. In the invisible maze task, participants wearing a wireless electroencephalography (EEG) headset were free to explore their surroundings, only given the objective to build and foster a mental spatial representation of their environment. Spatial uncertainty was resolved by touching otherwise invisible walls that were briefly rendered visible inside VR, similar to finding your way in the dark. We showcase the capabilities of mobile brain/body imaging using VR, demonstrating several analysis approaches based on general linear models (GLMs) to reveal behavior-dependent brain dynamics. Confirming spatial learning via drawn sketch maps, we employed motion capture to image spatial exploration behavior describing a shift from initial exploration to subsequent exploitation of the mental representation. Using independent component analysis, the current work specifically targeted oscillations in response to wall touches reflecting isolated spatial learning events arising in deep posterior EEG sources located in the retrosplenial complex. Single-trial regression identified significant modulation of alpha oscillations by the immediate, egocentric, exploration behavior. When encountering novel walls, as well as with increasing walking distance between subsequent touches when encountering novel walls, alpha power decreased. We conclude that these oscillations play a prominent role during egocentric evidencing of allocentric spatial hypotheses.

KEYWORDS

electroencephalogram, mobile brain/body imaging, single-trial regression, spatial cognition, virtual reality

Abbreviations: AMICA, adaptive mixture independent component analysis; ANOVA, analysis of variance; BEM, boundary element head model; cm, centimeters; EEG, electroencephalography; ERSP, event-related spectral perturbations; Hz, Hertz; IC, independent component; ICA, independent component analysis; LED, light-emitting diodes; MNI, Montreal Neurological Institute; MoBI, Mobile Brain/Body Imaging; ROI, region of interest; RV, residual variance; s, seconds; *SD*, standard deviation; TFCE, threshold-free cluster enhancement; VR, virtual reality.

Edited by: Daniel Ferris

1 | INTRODUCTION

Learning to predict the reward a given spatial challenge will yield, for example, estimating how to get to the grocery store to purchase food, is an integral part of daily activities. Assessing whether to take on a specific spatial task implies cost-benefit analyses where invested costs depend on the efficiency with which one can solve such spatial challenges. In modern times, GPS devices provide the ultimate navigational aid to solve these daily spatial challenges. However, the human spatial navigation system evolved largely without technical help and in widely different environmental conditions reinforcing distinct spatial strategies (Ishikawa & Montello, 2006; Loomis et al., 1993).

In order to reach the grocery store, the simplest strategy would be to "pilot" toward a cue indicating the store's location, for example, the smell of the hot-dog stand next to the store (Hamburger & Knauff, 2019). If the store is located several blocks away, this strategy becomes challenging. Following a previously learned sequence of actions derived from a preceding cue allows to successfully complete this task. In children, Jensen et al. first assumed an ontogenetic sequence from egocentric (self-to-object) to allocentric (object-to-object) representations (Hazen et al., 1978; Jensen et al., 1958; Siegel & White, 1975). In their words, the first stage of spatial knowledge entails encoding sensory representations of landmarks such as the hot-dog stand. Then, route knowledge develops through repetitive rehearsal and travel between previously encountered landmarks, a form of stimulus-response learning. Now, in the surprising situation where a fire truck blocks one street on the way to the store such a route strategy is bound to fail. Here, a flexible internal representation of the surrounding space provides the basis to choose among several paths and circumvent the obstacle. Different routes are connected to form a map-like model, survey knowledge. In short, survey knowledge, conceived in an allocentric reference frame, develops from the egocentric sensorium over repeated travels (for a critical discussion see Gramann, 2013; Ishikawa & Montello, 2006). Selecting an optimal path given changing criteria, for example, offering the most shade on a hot summer day, is possible based on a mental representation of the environment.

Tolman (1948) observed rats being able to exploit spatial knowledge acquired over repeated explorations of the same maze. He observed the rats take optimal detours en route to a food box with the direct path being blocked. He concluded that the rats' behavior was not explainable in terms of stimulus-response learning alone, but rather through the transition from exploration to exploitation. The rats must have learned an accurate spatial model, in other words, a "cognitive map."

Particularly, over the last decade, understanding cognitive processes such as spatial knowledge acquisition as a predictive process has gained substantial traction (Clark, 2013). Active inference posits perception as the imperative to minimize prediction error of the sensory consequences when actively sampling the hidden variables governing the behavior of the environment (Friston, 2010). In the natural physical reality, environmental affordances give rise to diverse behaviors including, for example, visual (grocery store sign) and olfactory (smell of the hot-dog stand) sampling but also reaching, grasping, and walking. However, traditional human brain imaging studies investigating the neural underpinnings of spatial navigation have almost exclusively relied on active visual sampling of navigationally relevant content or simplistic button movement control due to mobility restrictions of the neuroscientific methods.

With this paper, as well as a companion paper in the same issue (Miyakoshi et al., 2020), we challenge this limitation investigating the brain dynamics in actively behaving healthy human participants. Previously, we introduced the invisible maze task breaking down spatial knowledge acquisition to isolated, discrete, percepts, or "atoms of spatial thought." Here, we asked participants to form a spatial model of simple mazes, equivalent to survey knowledge or a cognitive map, and observed them during the early stages of the shift from exploration, ambiguity resolving, to exploitation, reward-seeking, behavior (Berger-Tal et al., 2014; Friston et al., 2016). Similar to navigation with a white cane, reaching and touching otherwise invisible walls briefly render the wall at the location of the touch visible. We hypothesized that spatial evidence is accumulated through repeated touching thereby emphasizing the interaction opportunities afforded by the environment in order for one to find its way through it (Gehrke et al., 2018). We simplify the ongoing predictive processes in our task as follows: First, hypotheses are generated about the sensory consequences of the next reach with respect to the location, orientation, and shape of the hidden walls. The reach to touch is acted out and subsequently, the sensory consequences of either a visual feedback, success, or the lack thereof, failure, are evaluated in light of a mismatch between what was the hypothesized action outcome and what was observed, that is, prediction error. Ultimately, back propagation of the prediction error across the hypothesis generation hierarchies, from simple proprioceptive to complex cognitive map hypothesis "generators," functions as the learning objective updating subsequent hypotheses. Therefore, in combination with ongoing brain and body imaging, continuous as well as event-related analyses of cortical dynamics of navigation and the context and environmental affordances under which they occur are feasible (Gramann et al., 2011, 2014; Jungnickel et al., 2019; Makeig et al., 2009).

To foster spatial learning as a transition from egocentric to allocentric spatial knowledge, in our *invisible maze task*, participants repeatedly explored the same mazes. Following each exploration, we assessed drawn sketch maps to quantify

spatial learning. We hypothesized a qualitative improvement with each additional exploration. In addition, we hypothesized changes in body dynamics to occur from formation to consolidation of spatial representations reflecting the function of cognition to optimize the outcome of behavior. Therefore, we hypothesized that the number of wall touches and time spent in mazes would be reduced and exploration velocity be increased as spatial representations become more accurate, possibly as a consequence of optimization of the energy costs of querying the spatial environment. Further, we hypothesized that participants focus on navigationally relevant maze characteristics in the later explorations indicated by prolonged time spent and higher numbers of wall touches occurring at these locations, further indicating more efficient behavior.

1.1 | Neural networks for spatial navigation

The neural cells, cortical structures as well as networks underlying spatial cognition have been well described (Burgess, 2014; Epstein et al., 2017; Ito et al., 2015; Moser et al., 2008; O'keefe & Nadel, 1979; Whitlock et al., 2008). Modeling spatial information integration provided further evidence about an interplay of a hierarchical network integrating multimodal sensations and mapping the sensory evidence to representations about the spatial environment (Byrne et al., 2007; Madl et al., 2015). The model by Byrne et al. (2007) is based on two spatial representations that utilize allocentric and egocentric reference frames. Allocentric maps, represented in the medial-temporal lobe, are fixed to distinct features in the environment, that is, landmarks and environmental boundaries (Epstein et al., 2017; Grieves & Jeffery, 2017). On the other hand, egocentric maps encode objects at a specific distance and in a specific head direction. The model specifies several modules representing both representation types and computing operations. A transformation module manifested in the retrosplenial cortex and driven by head-direction representations translates egocentric to allocentric map representations and vice versa (Mitchell et al., 2018; Vann et al., 2009). In their BBB model, Byrne et al. (2007) propose the "parietal window" metaphor modeling parietal computations as an egocentric view processing on long-term spatial memory to serve the demand for egocentric action. Along the dorsal stream, parietal cortex entertains connections to premotor areas and as such is well situated for an egocentric call-to-action serving navigational demands (Kravitz et al., 2011). Further, a demonstrated function in 3D depth perception as well as in temporal integration, that is, context, are functional prerequisites for directing egocentric reaching movements to sample the environment evidencing allocentric spatial hypotheses (Freud et al., 2016; Hohwy, 2016; Huk & Shadlen, 2005). With allocentrically coding cells abounding in medial-temporal structures, parietal cortex presumably concerts and binds the egocentric sensorium.

Positioned between deep medial temporal structures and parietal cortex, retrosplenial cortex is believed to sit at the conversion between allocentric and egocentric reference frames. Recently, Clark et al. (2018) argued for a relaxation in the understanding of a strict egocentric-allocentric parcellation of parietal and retrosplenial cortices. Reviewing the literature, they argue for a functional gradient from global allocentric coding in retrosplenial to egocentric and local allocentric coding in parietal cortex. In the current work, we directed our investigation to oscillations arising in or near the retrosplenial complex (Epstein, 2008; Gramann et al., 2018). Epstein (2008) coined the term retrosplenial complex due to the restricted anatomical differentiation of the retrosplenial cortex (BA 29 and 30) and the adjacent posterior cingulate (BA 23 and 31). We were interested in frequency band characteristics indicating spatial learning, and further, whether egocentric or allocentric processing express in specific frequencies.

First, based on previous observations in stationary spatial learning experiments (Chiu et al., 2012; Gramann et al., 2010; Lin et al., 2015; Plank et al., 2010), we investigated whether power changes in continuous theta and alpha oscillations exhibited spatial specificity during spatial learning. Following previous findings implicating these frequency bands in spatial cognitive processes in the retrosplenial complex, we hypothesized a modulation by spatial location within a maze. Theta activity in medial temporal, as well as deep parietal regions, has previously also been reported to emerge during *physical* spatial exploration, with a potential further modulation by movement speed (Bohbot et al., 2017; Liang et al., 2018; Snider et al., 2013; Yang et al., 2017). Importantly, hippocampal spatial prediction error signaling may travel in theta frequency (Stachenfeld et al., 2017). With the hippocampus potentially appearing as a predictive map, theta may carry top-down prediction error signaling through the hierarchy evidencing allocentric (spatial) hypotheses.

Alpha activity across parietal brain areas emerges in a wide range of functions (Klimesch, 2012). Specifically, relevant to spatial cognition, alpha activity has been measured during modulations of top-down, directed, spatial attention (Deng et al., 2019) in parietal cortex. As such it has frequently been observed during egocentric viewpoint changes, translations and rotations, in EEG studies targeting deep posterior sources during spatial tasks (Chiu et al., 2012; Gramann et al., 2010; Lin et al., 2015; Plank et al., 2010). Due to the novelty of sampling unconstrained, physically moving, and interacting navigators in our setup, no hypotheses regarding the directionality of effects on frequency bands were posited previous to data collection.

We followed up on the analysis of continuous oscillatory power modulations framed in spatial learning, by leveraging the promise of our paradigm breaking down spatial learning to isolated events. Therefore, event-related spectral perturbations (ERSPs) locked to the onset of a wall touch were analyzed and inspected as a function of repeated maze explorations as well as in a single-trial regression scheme to carve out spectral modulators of egocentric spatial behavior. While concentrating on previously observed theta and alpha modulation in posterior structures associated with egocentric and allocentric processing of spatial information, we used data-driven analyses to see whether additional frequency bands might reflect active spatial sampling in this new paradigm. Again, we hypothesized a change in activity as a response to spatial learning over repeated maze trials as well as immediate exploration behavior modulating activity in response to wall touches in the context of spatial learning.

2 | MATERIALS AND METHODS

2.1 | Participants, setup, task, and procedure

Thirty-two healthy participants (aged 21–45 years, mean = 28.8, *SD* = 6.6, 14 men) took part in the experiment. Participants were recruited through an online tool provided by the Department of Psychology and Ergonomics at TU Berlin and through local listings. All participants gave written informed consent to participation and the experimental protocol was approved by the local ethics committee (protocol: GR_08_20170428). Participants were compensated with 10 Euros per hour or study credits. All participants had normal or corrected to normal vision. Three participants were excluded from data analysis due to incomplete data or difficulties in complying with task requirements.

Participants were screened with regard to their spatial reference frame proclivity (Goeke et al., 2015; Gramann et al., 2005). This online available tool determines the proclivity of participants to preferentially use either an egocentric or an allocentric reference frame during a virtual path integration task. Of the 29 participants, 14 tested for an egocentric, 13 for an allocentric, and two for a mixed reference frame proclivity. No specific criteria were enforced for participant exclusion, other than being under the influence of performance-altering substances. To control for simulator sickness, potentially impacting task performance, the Simulator Sickness Questionnaire (SSQ) was administered twice, before and after the experiment (Kennedy et al., 1993). The SSQ measures simulator sickness on three factors: nausea, oculomotor, and disorientation. No difference between pre- and post-experiment exposure was noted, hence excluding simulator sickness as a covariate. Additional information and an in-depth description of the sample and the correlation structure between questionnaires and task performance can be found in Gehrke et al. (2018).

2.2 | Setup, motion capture, and EEG recording

Participants freely explored a sparse invisible maze environment interactively by walking and probing for visual feedback when touching the virtual wall of a 1 m wide path with their right hand. All stimuli were presented using an Oculus Rift DK2 virtual reality (VR) headset (Facebook Inc., Menlo Park, California, USA; 100∘ nominal field of view horizontally and vertically, 960 × 1,080 pixels per eye, 75 Hz frame rate). A rigid body composed of six red active light-emitting diodes (LED) was mounted to the headset and optically tracked via PhaseSpace Impulse X2 system (PhaseSpace Inc., San Leandro, CA, USA). To update the headset position, optical motion capture data were sampled at 240 Hz and smoothed by averaging across one frame update of the headset, approximately 13.3 ms. To correct orientation drifts originating from unstable inertial data, we continuously calculated an offset between the stable orientation of the motion capture rigid body and the unstable magnetometer data. Position and orientation of the right hand were tracked using a dedicated PhaseSpace glove with eight LEDs. Furthermore, four rigid bodies consisting of four LEDs each were attached to the lower arm, upper arm, and both feet. Visual stimuli were generated on a MSI (MSI Co. Ltd, Zhonghe, Taiwan) Gaming Laptop (MSI GT72-6QD81FD, Intel i7-6700, Nvidia GTX 970M) using WorldViz (Santa Barbara, California, USA) Vizard Software worn in a backpack. Participants were further equipped with a microphone and headphones for audio communication and masking of auditory orientation cues.

EEG data were recorded from 157 active electrodes with a sampling rate of 1,000 Hz and band-pass filtered from 0.016 to 500 Hz (BrainAmp Move System, Brain Products, Gilching, Germany). Using an elastic cap with an equidistant design (EASYCAP, Herrsching, Germany), 129 electrodes were placed on the scalp, and 28 electrodes were placed around the neck using a custom neckband (EASYCAP, Herrsching, Germany) in order to record neck muscle activity. Data were referenced to an electrode located closest to the standard position FCz. Impedances were kept below 10 kΩ for standard locations on the scalp, and below 50 kΩ for the neckband. Electrode locations were digitized using an optical tracking system (Polaris Vicra, NDI, Waterloo, ON, Canada). Motion capture and EEG samples were recorded and synchronized using labstreaminglayer (https://github.com/sccn/labstreaminglayer).

2.3 | The invisible maze task

Upon collision of the right hand with an invisible wall, a white disc was displayed 30 cm behind the collision point parallel to the invisible wall much like the beam from a torch in a cave, see Figure 1c. No other visual stimulation was presented inside VR. We did not track the left hand and instructed participants to keep the left arm close to their body. Prior to the first trial, participants were familiarized with the VR scene. To this end, participants were placed in front of a virtual wall and were guided through experiencing the full interactivity of the scene, that is, touching and drawing. When a satisfactory understanding of the interaction possibilities was apparent, participants were asked to take a couple of steps along the wall while touching it to their right-hand side to train the desired task behavior.

Performing the task, participants explored four different mazes in the order, "I," "L," "Z," and "U" in three consecutive trials for each maze (see Figure 1b). For each maze, the procedure was as follows: participants were briefly disoriented and then positioned facing the open side of the path. Then, participants were directed to explore the invisible path until they reached a dead end, and subsequently find their way back to the starting position. At the end of each maze and trial, termed "maze trial," participants received a gamified feedback and were then asked to draw a sketch map of the maze from a bird's eye view. Therefore, participants remained inside VR and an experimenter entered the lab space and handed the participant a computer mouse to control the drawing application. Participants were instructed to start drawing by clicking once with the left mouse button. A red sphere appeared in the VR goggles at the tracked position of the right hand holding the mouse. Holding down the left mouse button, participants were able to draw a red line by moving their hand in space (see Figure 1d). Finally, participants were instructed to take a camera screenshot of their drawing by pressing down the mouse wheel once and holding their final drawing in view. Participants were allowed to erase their drawing and restart at any time by pressing the right mouse button.

The whole procedure was repeated three times in a row for each maze to foster spatial learning within each maze. Between mazes, participants had the opportunity to take a brief break and were made aware of the change to a new maze. The complete experiment, including preparation of physiological measures (electroencephalogram, EEG), took approximately 4 hr. Preceding and following the task, participants completed a set of questionnaires. In this paper, we report how perspective-taking ability as well as self-ascribed sense of direction impacted drawing of sketch maps. In the Perspective Taking and Spatial Orientation Test (PTSOT), participants viewed an array of objects on a sheet of paper and by taking the perspective of one of the objects judged the angle between two other objects in the array (Hegarty, 2002). We recorded the absolute deviation from the correct angle to investigate the impact of perspective-taking ability. The Santa Barbara Sense of Direction Scale (Freiburg Version), FSBSOD, measures self-ascribed navigational ability (Kozhevnikov & Hegarty, 2001). We took the average of all items as the final measure.

2.4 | EEG preprocessing, independent component analysis, and motion capture preprocessing

Electroencephalography data preprocessing and independent component analysis (ICA) were performed with

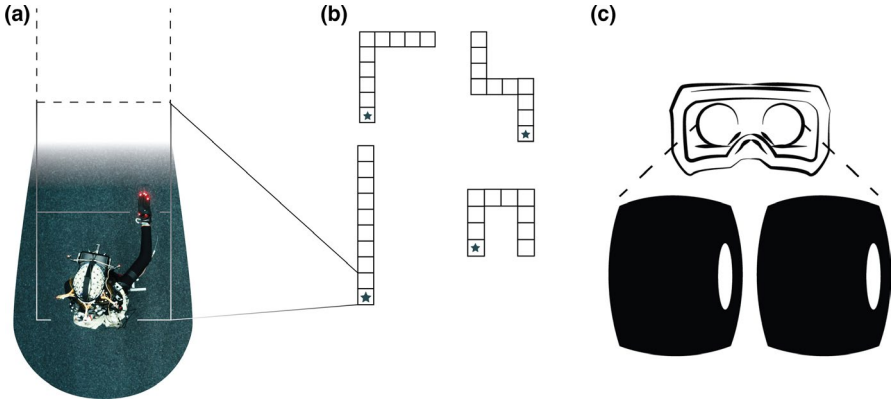

FIGURE 1 (a) Participant displayed from a bird's eye view located at the starting point of an "I"-maze. The star marks the starting position but was not visible during the experiment. Participants were instructed to explore the maze and return to the start after full exploration of the maze. (b) Four mazes were used in the study including an "I," "L," "Z," and "U" shaped maze clockwise from lower left to lower right. Each maze was explored three times before the next maze was learned. (c) Exemplary visual feedback in first-person view in binocular "VR optics" of subject in A (above) touching the wall to the right. No other visual stimulation was presented inside VR. This figure is in part licensed CC-BY and available in color on Figshare (Gehrke et al., 2018)

MATLAB 2017a and 2019b (MATLAB, The MathWorks Inc., Natick, MA, USA), using the EEGLAB toolbox (Delorme & Makeig, 2004) and the custom "BeMoBIL Pipeline" scripts and functions.[1] The single subject data were low-pass filtered with 124 Hz and subsequently down-sampled to 250 Hz. An average of 12.7 (SD = 2.8) noisy channels were identified and removed through manual inspection on the time domain. Rejected channels were then interpolated while ignoring the EOG channel, and finally re-referenced to average reference (data A). The data were then filtered with a 1 Hz high-pass filter (data B) and a first single-model adaptive mixture independent component analysis (AMICA) (Palmer et al., 2011) was used to identify eye-related independent components (ICs), which were projected out of the sensor data. For this, the rank was reduced by one for the use of an average reference and further by the number of interpolated channels in the respective dataset. To identify eye components, ICLabel (Pion-Tonachini et al., 2019) was used, with components exceeding a value of 0.5 for the "eye" class being defined as eye components. Then, to detect segments of noisy data across channels, an automated time domain cleaning (see Gramann et al., 2018) was performed on narrowly filtered data (data B) from 1 to 40 Hz. The data were therefore first split into 1-s-long segments for which the mean absolute amplitude and standard deviation of all channels as well as the Mahalanobis distance of all channel mean amplitudes were calculated. Results of all three methods were then joined together in order to rank all segments. The 12% highest ranking noisy segments were selected for rejection and an additional buffer of ±0.49 s was added around each segment resulting in about 15% rejected data for each subject. These data were rejected from data B and a second single-model AMICA was calculated on this time domain cleaned data. A dipole fitting procedure was performed for each spatial filter using the 10–20 standard electrode locations and a boundary element head model (BEM) based on the MNI brain (Montreal Neurological Institute, MNI, Montreal, QC, Canada) using dipfit routines (Oostenveld & Oostendorp, 2002). The spatial filter information and equivalent dipole models were then copied back to the pre-processed, interpolated, and average-referenced dataset (data A). Ultimately, all ICs with a "brain" probability smaller than 0.5 as indicated by ICLabel were projected out of the data resulting in the final dataset of likely brain sources and their projections to the channels investigated in all subsequent analyses. Across the study set, 213 ICs were retained forming a sample of 7.3 (SD = 3.8) components per participant. Motion capture data were filtered with a 6 Hz zero-lag low-pass FIR filter and upsampled to match EEG frequency using MobiLAB routines for concurrent analyses (Ojeda et al., 2014).

[1]https://github.com/MariusKlug/bemobil-pipeline

2.5 | Clustering independent components for group-level analyses

To allow for group-level analyses across ICs, we clustered components based exclusively on their equivalent dipole locations, avoiding circular inference (Kriegeskorte et al., 2010). To this end, we employed our region of interest (ROI)-driven repetitive k-means clustering approach (Gramann et al., 2018). ICs were clustered by applying the k-means algorithm with k equal 10 for 10,000 times. ICs with a distance of more than three standard deviations from any final centroid mean were considered outliers. Similar to Gramann et al. (2018), we set the target clustering location to [0, −45, 30] in MNI space. From each of the 10,000 solutions, the cluster with a centroid closest to the target location was selected. Subsequently, the 10,000 selected clusters were ranked via weighting of the cluster's parameter. After applying desirable weights (number of participants: 3, ICs/participants: −2, spread: −1, RV: −1, distance from ROI: −2, Mahalanobis distance from the median: −1), the final clustering solution contained 30 ICs from 22 participants, that is a ratio of 1.3 ICs per participant and a mean RV of 7.9%. Following the assumptions of our clustering approach, which finds an optimal cluster for the given weights, we chose to average IC activity of participants exhibiting more than one IC in the optimized cluster wherever applicable.

2.6 | Analyses and statistics

Prior to the statistical analysis, the data were further pruned. The objective was to keep trials comparable across trials and participants. Trials of maze exploration with more than 10 wall collisions were rejected as such exploration behaviors likely reflected participants being stuck "outside" of the maze and not finding their way back into the maze on their own. The number of such trials was very low (six of a total of 348 maze explorations from 29 subjects exploring four mazes three times each). We further rejected four individual explorations because of technical issues (empty battery of the LED driver or loose LED cable). Central for a comparison of trials in which participants were able to build a spatial representation of the entire maze, we further deemed all explorations incomplete where the path was not fully explored as such trials indicated that participants turned around before reaching the dead end and could not build an adequate spatial representation of the maze. With this criterion, 26

explorations were rejected. Overall, 312 maze explorations remained, amounting to 89.7% of the total number of explorations.

2.7 | Behavior: Grand averages of sketch map, time-on-task, and number of touches

2.7.1 | Sketch map

Two independent raters judged each sketch map drawing. The raters were presented with the question: "Imagine that you can take the present sketch map with you into the virtual environment and use it as a navigational aid. How useful would the map be for you?" To give their rating between 0 (= no help at all) and 6 (= very helpful), they were given the correct shape of the maze to be rated, see for example Figure 1b top left "L" shape, side by side with the drawing to rate, see exemplary "L" sketch maps in Figure 2b. To test inter-rater reliability, we computed Cohen's Kappa with squared weights to emphasize larger rating differences using RStudio Version 1.2.5001 (RStudio Team, 2019; RStudio, Inc., Boston, MA, USA) and package irr (Cohen, 1960; Gamer et al., 2010).

2.7.2 | Time-on-task, number of touches, and velocity

Using motion capture, we extracted the time elapsed between the start of each maze trial and the return to the starting position as well as the total number of wall touches during that time window. Reported velocity refers to the magnitude in 2D (ground plane) of the head rigid body. When considering maze complexity, we refer to the number of turns afforded by a maze.

Due to unbalanced data after cleaning with respect to the factorial design, group-level statistics of behavioral data were performed using linear mixed effects model with package lmerTest (Kuznetsova et al., 2017). For each measure: sketch map, time-on-task and number of touches, a linear mixed effects model with fixed effects for Maze and Trial, their interaction and the random effect of participant was fit. Post-hoc contrasts were computed using package emmeans with Tukey's correction for multiple comparisons (Lenth et al., 2020).

2.8 | Behavior: Mapping head location at wall touches

To increase the resolution of the exploration behavior, we constructed 2D "bird's-eye view maps" indicating where participants were located when touching a wall. Therefore, for each maze and trial, a 2D histogram with fixed edges, in order to maintain equal resolution across participants, was computed using the (x, y) head location at the times of the wall touches. To increase overlap across participants, a 2D (square sized) Gaussian blur was applied to the resulting histogram image. A σ of 2 was chosen for the 2D filter kernel as it resulted in a good overlap across participants while maintaining spatial specificity. Group-level statistics on the images were performed using MATLAB functions fitrm and ranova. The analysis was conducted for each maze independently due to the shape differences of the mazes. For each pixel, a 1 × 3 repeated-measures ANOVA was conducted across the three trials within subjects. At each pixel, we removed all missing data (see description of the cleaning procedure above) and only conducted model-fitting if data from more than 12 participants were available. Else, the pixel was set to NaN. We corrected for multiple comparisons using false discovery rate (Benjamini & Hochberg, 1995) at $\alpha = 0.05$. We report both corrected and uncorrected significance masks due to the exploratory nature of the study. To report results, we extracted the F statistic and post-hoc contrasts at a given pixel of interest. For visualization purposes, we removed all patches including less than 2 significant pixels.

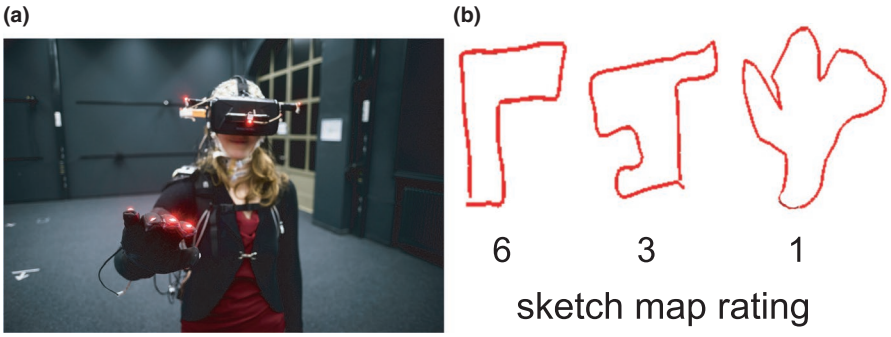

FIGURE 2 (a) Participants wore high-density wireless EEG, head-mounted virtual reality goggles, and LEDs for motion capture attached to the hands, goggles, and torso. (b) Screenshot of drawn sketch maps of maze L. Three map drawing examples ranging from good (left, rating 6), to intermediate (middle map rating 3), to bad (right, rating 1)

2.9 | EEG: Spectral maps

To address whether spectral activity of clusters of independent EEG components exhibited spatial specificity during maze exploration, images of spectral activity were constructed at each location (x, y). Therefore, we first computed the power spectral density for moving windows of 1 s length with a step size of 0.2 s between the start and end of each trial using EEGLAB's spectopo function. For computational purposes, we subsequently subsampled motion capture and power data at 1 Hz. In case a subject exhibited more than one IC in the cluster, the power values were averaged across participants. As above, a 2D histogram of the motion capture data with fixed edges per maze was constructed and for each histogram bin, power data were averaged and blurred with a Gaussian with a σ of 2 to increase overlap across participants. Subsequently, maps of individual frequencies (theta 4–8 Hz and alpha 8–13 Hz), trials, and mazes were normalized dividing each map by its mean and subsequently transforming the image values to logarithmic scaling (dB = 10 × log10(power)). Group-level statistics were performed in identical fashion to the head location maps. For plotting purposes, grand averages were first obtained in power and subsequently baseline corrected and transformed to logarithmic scaling.

2.10 | EEG: Event-related spectral perturbations at wall touches

For each IC present in the cluster of interest, data were epoched −1 to +3 s around the wall touch event. First, epochs were rejected if the touch duration was longer than 2 s, that is, resulting in a warning signal appearing in the VR where the disc turned red, see Gehrke et al. (2018) for details. The remaining epochs were subjected to a cleaning routine identifying considerable artifacts in the IC activation time course based on epoch mean, standard deviation, and Mahalanobis distance (Gramann et al., 2018). Per participant, the worst 10% epochs were flagged for removal. On average, 723 (SD = 334) epochs remained for further analysis. Time-frequency decomposition was computed via the newtimef function in EEGLAB for 3–80 Hz in logarithmic scale, using a wavelet transformation with three cycles for the lowest frequency and a linear increase with frequency of 0.5 cycles. As participants' behavior was not restricted, wall touches could be of different duration. Therefore, we calculated time-warp anchors across all touches (mean touch duration = 700 ms) and ERSPs were linearly warped to the touch onset (0), the end of the touch (700 ms), and 700 ms succeeding the end of the touch (1,400 ms). Subsequently, phase was discarded, and power values were kept for further analysis. To obtain baseline power spectral density vectors, power values preceding touch events (from −400 to −100 ms) were averaged across time. In case a subject exhibited more than one IC in the cluster, the ERSPs were averaged.

2.11 | EEG: ERSP condition average statistics

Statistics on the grand-average ERSP were computed using statconds permutation t-test with 1,000 permutations. For each participant, averaged epochs as well as baseline power were aggregated. Next, the baseline vector was repeated to match the epoch size in time. Permuting epochs and baseline for 1,000 times and computing t-tests result in the distribution under the null hypothesis. To assess statistical significance, the true result was thresholded at $\alpha = 0.05$ against the null distribution. We corrected for multiple comparisons using false discovery rate (Benjamini & Hochberg, 1995) at $\alpha = 0.05$. For grand average plotting, participant power averages were aggregated (mean) and subsequently, data of the grand average touch epoch were divided by the baseline vector and the outcome was transformed to logarithmic scaling (dB = 10 × log10(power)). Final plots contain the significance thresholds as contours of significant time-frequency bins. For plotting purposes, significant patches exhibiting less than 50 pixels were removed and the significance mask was filtered using a Gaussian with $\sigma = 1.5$.

Group-level statistics for maze, trial, and their interaction were performed using robust repeated-measures ANOVA as implemented in LIMO EEG (Pernet et al., 2011). First, data from one participant were removed due to missing data. Then, epoch as well as baseline power were aggregated (mean) for each maze and trial. Subsequently, power data of the touch epochs were divided by the baseline vectors and the outcome was transformed to logarithmic scaling (dB = 10 × log10(power)). To assess effects, family-wise error rate (FWER) was controlled using threshold-free cluster enhancement (TFCE) as implemented in LIMO EEG. Due to the small sample size (N = 21), only bootstraps containing more than 70% of subjects were considered for the max-TFCE distribution (Pernet et al., 2015). The threshold was set at $\alpha = 0.05$ of a max-TFCE distribution of 600 bootstraps. As before, we report both uncorrected as well as corrected p-values. For plotting purposes, significant patches exhibiting less than 10 pixels were removed.

2.12 | Post-hoc EEG: ERSP single-trial analysis

Following up our analysis on condition averages, we considered the information present in the head location maps

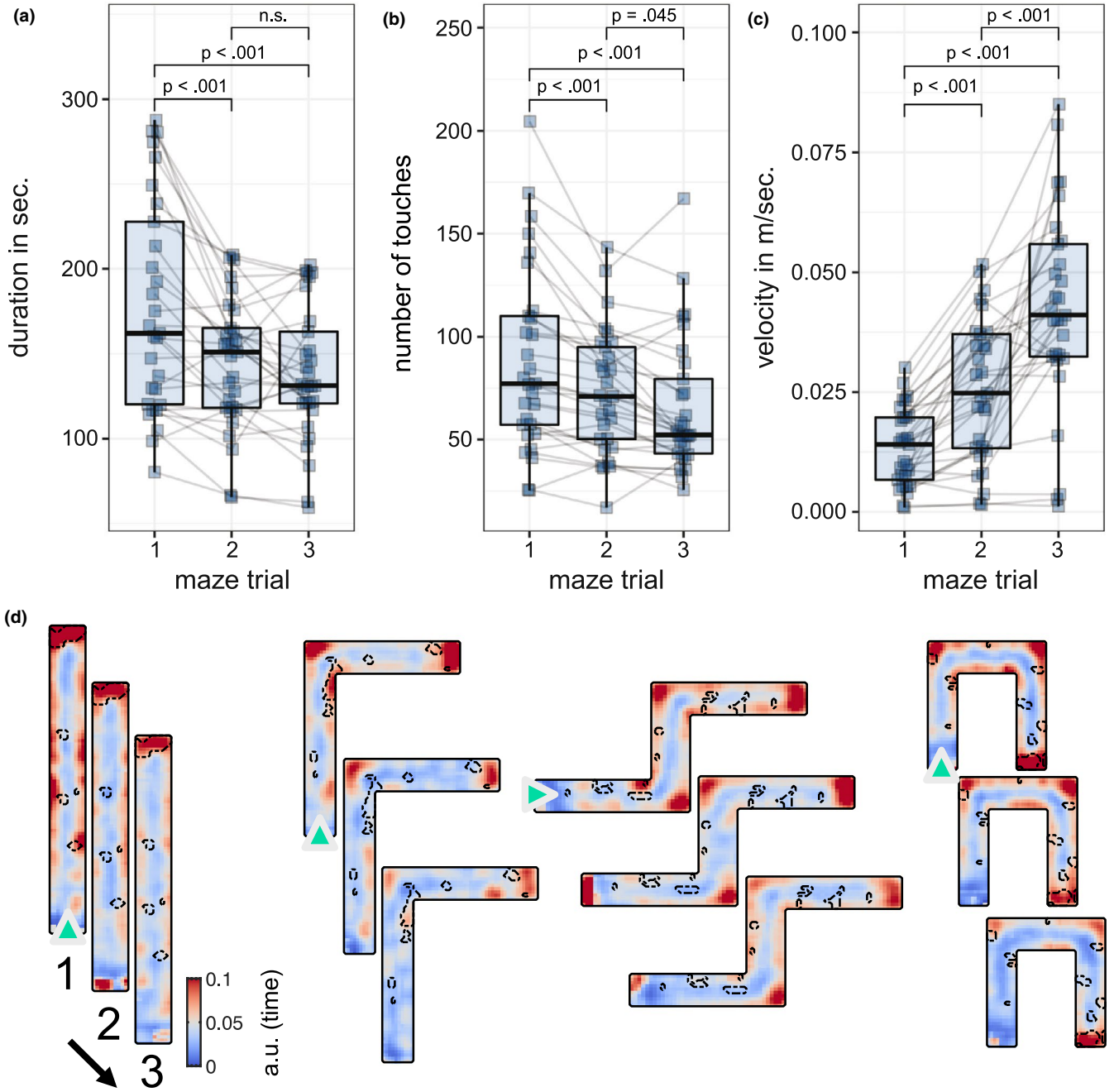

FIGURE 3 Top row: Box-Whisker plots with individual observations of each participant averaged across maze configurations for each repeated maze trials 1–3. (a) Duration in seconds elapsed between the start and end of each exploration phase, (b) Number of wall touches during the exploration phase, and (c) Movement Velocity in meters per second. (d) 2D histograms of the head location at wall touch moments for all three explorations in each maze "I," "L," "Z," and "U." Warmer colors indicate more wall touches/time spent at location. Solid (corrected) and dotted (uncorrected) contours mark significant pixels of repeated explorations

and derived the following single-trial analysis scheme. We considered the distance participants traveled between touches in combination with the encounter of a new versus an old wall as efficiently separating the touching behavior in corners versus along straight segments. There, we first computed the distance traveled since the previous successful touch, the Euclidean norm between two succeeding touches. To obtain per participant summaries of ERSP, mass-univariate multiple regression was computed. A linear model was estimated at each time-frequency pixel. The linear model was defined as tf_pixels = intercept + distance_traveled × wall_change + baseline. In order to estimate the interaction term, both predictors were z-scored prior to model fitting. To further infer whether components of the event-related response could be explained by baseline activity, baseline power was entered as a predictor. To assess effects, statconds one-sample permutation *t*-test with 1,000 permutations were computed

using the betas per participant. Subsequently, the surrogate *t*-tests were transformed to the TFCE statistic (Pernet et al., 2015). The threshold for multiple comparison was set at $\alpha = 0.05$ of the max-TFCE distribution of 1,000 permutations. For plotting purposes, significant patches exhibiting less than 10 pixels were removed.

3 | RESULTS

3.1 | Behavior

The sketch map usefulness ratings revealed a very high agreement between the two raters' judgments, Cohen's $\kappa = 0.835$, $p < 0.001$. Participants drew useful sketch maps already after the first maze trial (intercept: $t_{124.5} = 9, p < 0.001$; see Figure 2 for exemplary sketch maps and their average usefulness rating). On average, 2/3 were able to draw very useful sketch map, see Figure 7, with the remaining third exhibiting an average sketch map rating of less than 2, referring to a sketch map that is of little help as a navigational aid. With repeated maze explorations, ratings of the usefulness of the drawn sketch maps did not further improve ($F_{2,271.3} = 1.8, p = 0.16$, mean first 3.2, $SD = 2.1$, second 3.6, $SD = 1.9$, and third trial 3.7, $SD = 1.9$), nor did they vary as a function of maze complexity ($F_{3,272.25} = 1, p = 0.4$, mean "I" 3.6, $SD = 2.1$, "L" 3.7, $SD = 1.8$, "Z" 3.3, $SD = 2.1$, and "U" 3.3, $SD = 1.9$) and their interaction. We confirmed that individual differences in spatial ability had an impact on the sketch map drawings. Increasing perspective-taking and spatial orientation ability, as assessed with the PTSOT questionnaire, positively impacted the rating of sketch maps ($b = 0.02$, $F_{1,27} = 4.9$, $p = 0.036$, $R^2 = 0.15$). We observed no impact of the subjective Santa Barbara Sense of Direction Scale on sketch map quality. As previously reported in Gehrke et al. (2018), we observed a decrease in time-on-task with repeated explorations ($F_{2,271.8} = 17.6, p < 0.001$) and a main effect of maze complexity, operationalized by the number of turns in the maze. More specifically, time-on-task decreased significantly comparing the first and second ($t_{272} = 4.47, p < 0.001$), as well as the first and third trials ($t_{272} = 5.57, p < 0.001$; see Figure 3a). The number of wall touches decreased with repeated explorations ($F_{2,271.1} = 26.1, p < 0.001$) with a significant decrease from first to second ($t_{271} = 4.63, p < 0.001$), first to third ($t_{272} = 7.01, p < 0.001$) as well as second to third ($t_{272} = 2.4, p = 0.045$) trial (see Figure 3b). Furthermore, participants moved faster with increasing explorations ($F_{2,272.35} = 46.1, p < 0.001$; see Figure 3c), as well as in simple compared to more complex mazes ($F_{2,274.1} = 6.8, p < 0.001$). However, no interaction effect was observed. The main effect of maze complexity on velocity was driven by the "I" maze, with significant linear contrasts between the "I" maze and all other mazes, for example, "I" – "U" ($t_{276} = 4.23, p < 0.001$).

To further investigate participants' exploration behavior, head locations were mapped at moments of wall touches indicating that participants sampled corners and dead ends more frequently than straight segments (see warmer colors in Figure 3d). Specifically, at the dead-end of the "I" maze ($F_{2,28} = 6.1$, $p = 0.005$ uncorrected) and "U" maze ($F_{2,28} = 18.9, p < 0.001$, FDR corrected), a decrease in the number of touches was observed as a main effect of trial. Furthermore, a change in touch frequency was observed at the inside turn in the "L" maze ($F_{2,28} = 5.6, p = 0.001$ uncorrected), trending down from earlier to later trials.

Taken together, participants took less time exploring the mazes in repeated explorations, needed fewer wall touches, and moved faster, Figure 3a–c. In detail, we observed participants spending most of their time exploring "outside" (convex) corners and in the dead ends, Figure 3d. This exploration pattern was largely unaffected by repeated explorations.

3.2 | Oscillations of independent EEG sources located in or near retrosplenial complex

Clustering ICs resulted in a cluster with a centroid location around X = 3, Y = −52, Z = 24 (MNI), a mean residual variance of 7%, containing 22 of 29 participants and 30 ICs, see Figure 4a. The MNI coordinates refer to the posterior cingulate bordering on the precuneus in the AAL atlas and BA23 (posterior cingulate cortex) in the Brodmann atlas, respectively.

Mapping continuous spectra to spatial locations revealed a main effect of repeated maze trials on theta band activity at the dead end of maze "I" ($F_{2,42} = 12.3, p < 0.001$), see Figure 4b top left, with the first trial exhibiting a higher power increase over its baseline then the subsequent trials two and three. Similarly, at the dead end of maze "I," alpha power was affected by repeated maze trials ($F_{2,42} = 13, p < 0.001$), see Figure 4b bottom left. Further patches of a main effect of repeated explorations were observed for maze "I" at the center of the maze path as well as toward the left wall (left from the starting position) in both theta and alpha frequency bands. For the other mazes, repeated explorations did not impact continuous theta nor alpha spectral power following correction for multiple comparison. Not correcting for multiple comparisons, mazes "L," "Z," and "U" exhibit slight effects of maze trial at the first turn segments ("L" and "U") as well as at the second turn ("Z") in the theta frequency band, see Figure 4b top. Overall, visual inspection hints at a concentration of power increase over the full-trial baseline at corners and dead ends in later compared to earlier trials and more so in theta than alpha frequency (see for example Figure 4b top "Z" and "U" mazes).

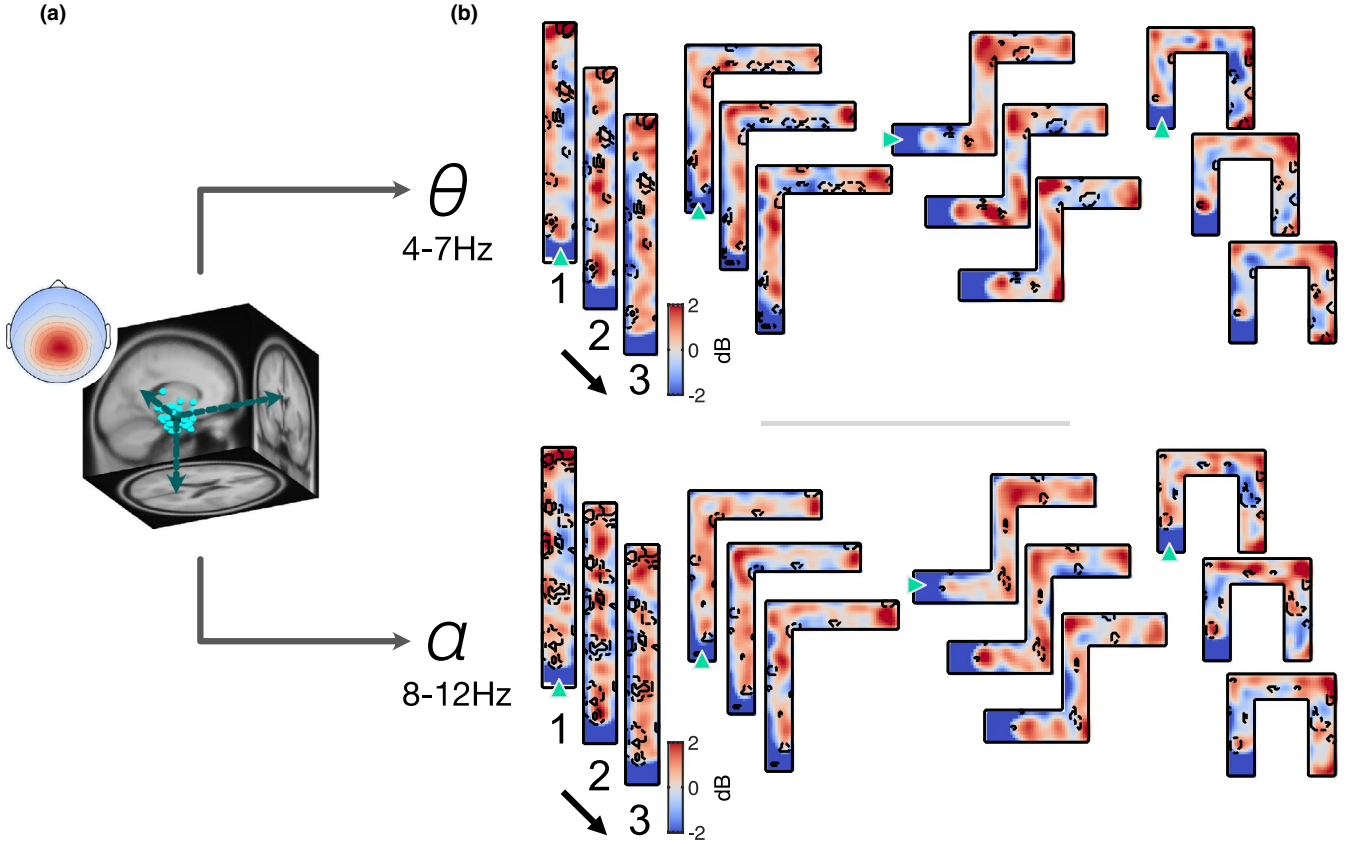

FIGURE 4 (a) Locations of equivalent dipole models projected onto a standard brain space (MNI) with each small sphere representing individual ICs and the bigger sphere representing the cluster centroid. The cluster centroid was located in retrosplenial complex (x = 3; y = −52; z = 24), containing 30 ICs from 22 participants (corresponding to 74% of all participants). (b) Images of theta (4–7 Hz, top) and alpha (8–12 Hz, bottom) power for all three explorations in each maze "I," "L," "Z," and "U." Warmer colors indicate higher power. Solid (corrected) and dotted (uncorrected) contours mark significant pixels of repeated explorations

3.3 | Zooming in: Event-related spectral perturbations to wall touches

Grand-average ERSP to wall touches differed from baseline power in theta, alpha, and beta band frequencies, see Figure 5a. Following onset of the visual feedback during the wall touch, an initial theta power increase ($t_{28} = 2.6$, $p < 0.001$ at 380 ms and 5.5 Hz) preceded significant alpha and beta desynchronization ($t_{28} = -2.6$, $p < 0.001$ at 630 ms and 12 Hz; $t_{28} = -3.3$, $p < 0.001$ at 600 ms and 24 Hz). Following the retraction of the hand from the wall, significant alpha and beta desynchronization persisted for another 400 ms. Repeated measures ANOVA of repeated trials did not impact wall touch ERSP following multiple comparison correction (see Figure 5b).

3.4 | Follow-up: Toward single-trial contextual analyses of spatial evidence integration

Figure 6b displays beta weights from single-trial regression including a baseline (bottom row), walking distance between subsequent wall touches, whether a new wall was encountered with the current touch, and their interaction as predictors. The interaction term (see Figure 6c) alludes to the fact that walking distance was on average greater when touching a new wall (mean = 57 cm, *SD* = 61) than following along the same wall (mean = 24 cm, *SD* = 33). As expected, baseline power impacted ERSP across all analyzed frequencies.

With increasing walking distance from the previous touch, alpha power increased throughout the duration of the touch event, for example, around 11.5 Hz and 350 ms following the visual onset of the touch feedback ($t_{22} = 2.7$, $p < 0.001$), see Figure 6b top left. At an uncorrected level, a positive relation was further observed for low frequencies (3–5 Hz) during (centered at 350 ms during the touch) as well as following the completion of the touch event. Touching a new wall, different to the one previously encountered, also positively affected low frequencies (3–5 Hz during the touch, $t_{22} = 3.7$, $p < 0.001$ at 200 ms and 3 Hz). Furthermore, albeit at an uncorrected level, alpha power was decreased in touches toward a wall different than the one previously touched. This pattern was visually conspicuous during the touch as well as following the touch event. Ultimately, the interaction term negatively impacted alpha

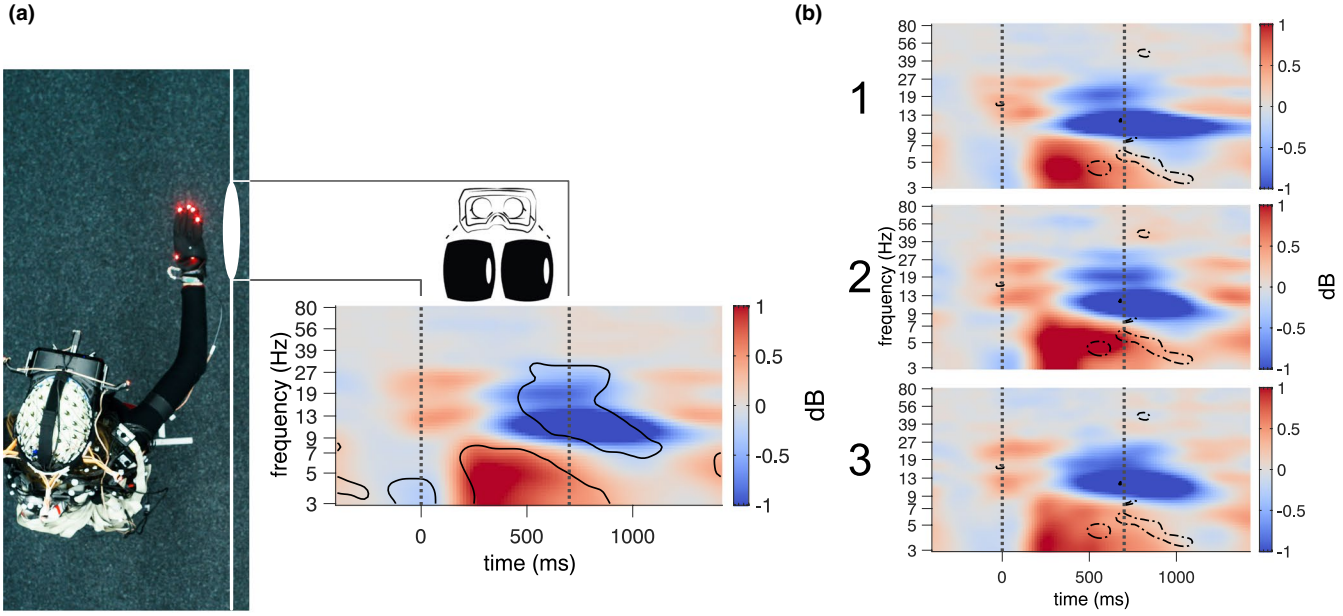

FIGURE 5 (a) Left: Magnification of bird's eye view of exemplary reaching to touch a wall. Touching a wall was visually indicated by a white sphere appearing oriented along the wall. Right: Grand-average "wall touch" ERSP in dB scale. ERSPs were linearly warped to the touch onset and mean offset (mean touch duration) and to 700 ms succeeding the touch. Solid (corrected) contours mark significant pixels compared to baseline. (b) Condition average ERSP per run aggregated across mazes, warmer colors indicate a power increase compared to baseline. Dotted (uncorrected) contours mark significant pixels of repeated explorations

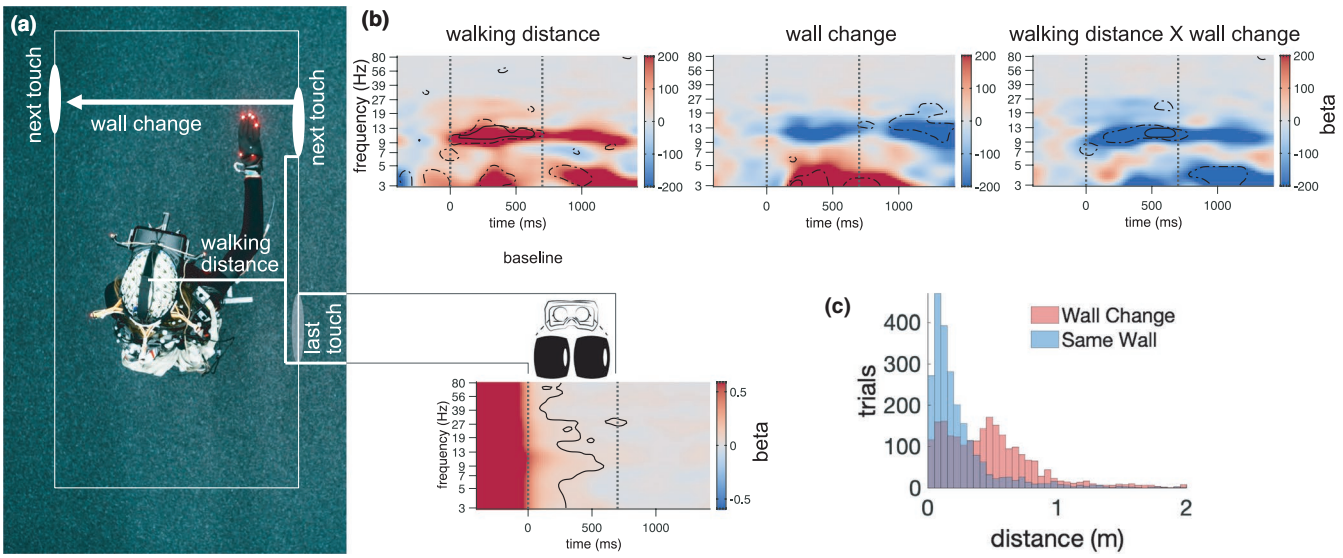

FIGURE 6 (a) Bird's eye view of exemplary reaching to touch a wall. Predictor "walking distance" refers to the distance the participant's head traveled between subsequent touches, predictor "wall change" indicates a touch to a different wall than the previous touch. (b) Top: Beta weights of single-trial linear regressions. Warmer colors indicate positive betas. Solid (corrected) contours mark significant pixels. Bottom: Beta weights of baseline vector. Visual feedback to wall touches was displayed as white spheres indicating walls in VR. (c) Histogram of "walking distance" split by factor "wall change"

power during the touch event ($t_{22} = -3.3$, $p < 0.001$ at 550 ms and 11.5 Hz), meaning with increasing walking distance and specifically only in touches toward a wall different than the one previous touched, alpha power was negatively affected. Furthermore, at an uncorrected level, power in low frequencies (3–5 Hz) was negatively impacted by the interaction term.

4 | DISCUSSION

We performed a mobile brain/body imaging (MoBI) study allowing physical full-body movement with which participants explored invisible mazes with the aim of building a mental model of the environment. Following a previous description

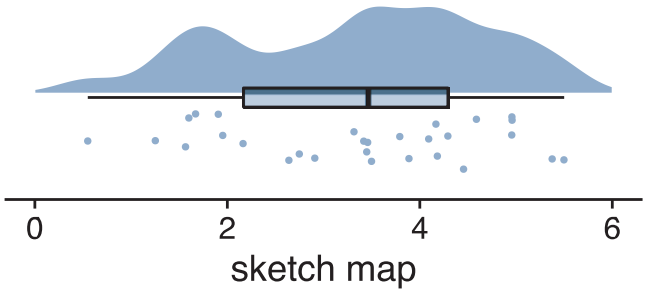

FIGURE 7 Distribution of participants' mean sketch map ratings across mazes and explorations. Ratings refer to the question: "How useful would the map be for you?" 0 (= no help at all) and 6 (= very helpful)

of behavior in this paradigm in Gehrke et al. (2018), we here explored EEG perturbations during spatial learning depending on hand thrusting movements to explore the environment. Our analyses specifically targeted deep posterior brain structures, in or near the retrosplenial complex. Here multimodal sensory signals from the "parietal window" converge with spatial memory, or predictions, originating from medial temporal structures such as the hippocampus (Clark et al., 2018; Stachenfeld et al., 2017). The data were analyzed in a repeated measures design manipulating spatial learning as well as a single-trial regression approach dissecting egocentric sampling of the surrounding space.

First, we confirmed successful manipulation of spatial learning by finding that participants explored *invisible mazes* in less time, with fewer touches and with overall increased exploration speed in subsequent trials. Furthermore, about 2/3 of participants were able to draw an accurate sketch map, demonstrating the formation of survey knowledge in an allocentric reference frame. Second, we introduced a novel way to report continuous spectral power by mapping theta and alpha band activity. Power in either frequency band and spatial location did not change significantly with repeated maze trials. Similarly, we investigated ERSP locked to wall touch events and did not observe significant modulation as a function of repeated trials. Meanwhile, compared to a pre-wall touch baseline, theta, alpha and beta activities were significantly modulated exercising the wall touches. Lastly, we disentangled wall touch ERSP by means of mass-univariate single-trial analysis and found a robust effect of alpha power increase with increasing distance traveled between consecutive touches. A decrease in alpha power in response to the encounter of novel walls was visually conspicuous but not significant. However, alpha power was decreased for the interaction, meaning it was decreased with increasing travel distance when encountering a new wall.

4.1 | Behavioral evidence of spatial learning

Although participants navigated with greater efficiency in all subsequent trials following the initial exposure, a continuous learning effect determined via sketch map quality was absent. On average, participants were able to draw useful sketch maps with a mean rating of 3.2 indicating the maps as "somewhat useful as a navigational aid." These maps, however, were either produced already following the first maze trial or participants were not able to draw a map at all. Sketch map quality did not change with repeated trials or as a function of maze complexity. Hence, underscoring previous findings, we confirmed that some participants were able to produce a useful map already after the first trial and then through all trials, whereas others never produced a useful sketch map at all (Weisberg & Newcombe, 2018), see Figure 7. Interestingly, in our companion paper, Miyakoshi et al. (2020) report identical effects in a similar invisible maze task based on auditory feedback to wall touches. In their work, however, only ~40% of participants were able to draw a map with topological similarity to the explored maze, shedding further light on the importance of individual characteristics as a precursor for formation of a cognitive map.

The importance of individual predispositions was further underlined by the fact that participants scoring high in perspective-taking ability (PTSOT) were more likely to draw useful sketch maps. Strongly related to mental rotation ability, perspective taking has also been linked to real-world navigation performance (Schinazi et al., 2013). In contrast, self-ascribed sense of direction did not exhibit any impact on sketch map production. Whether and how these predispositions impact spatial exploration behavior and EEG signals is an open question for future investigation.

We observed a discrepancy between the quality of sketch maps and the ability of nearly all participants to solve the task with increasing efficiency as reflected in decreasing time-on-task, number of wall touches, and increasing movement velocity over trials (Figure 3a–c). We hypothesize that those participants drawing useful sketch maps could also have made use of this allocentric representation during subsequent navigations, whereas the remaining participants may have solved the task more efficiently by increasing the accuracy of learned stimulus-response associations, for example, learning to take a certain number of steps after encountering a turn. Other approaches to assess allocentric spatial knowledge, such as distance and angular judgments, could prove fruitful in quantifying spatial knowledge in future experiments (Starrett & Ekstrom, 2018).

Although the evidence is scattered, we argue to have triggered spatial learning on the continuum from stimulus-response, or route knowledge, to allocentric survey knowledge, or cognitive map. Using motion capture to image exploration behavior, we further indicate that participants spend more time at presumably navigationally relevant sections in later trials with the frequency of wall touches concentrating in corners and dead ends (Figure 3d). Already within the first maze trial, participants sampled the walls in corners

and dead ends with a higher frequency than along straight segments. In terms of spatial microgenesis, corners and dead ends might have been integrated already during this initial exposure as distinct landmarks fostering stimulus-response associations.

Due to the invariant order of learning mazes from low to higher complexity levels, operationalized by the number of afforded turns, a continuous familiarization effect to the overall task might have masked maze-specific effects. This cannot be attributed to learning the interaction with the invisible maze as participants were trained prior to the first trial on the interactions afforded by the invisible walls. Hence, the first trial participants were familiar with the interaction and how to solve the spatial task. Nonetheless, we observed the "I" maze driving behavioral effects, with the first exposure to the "I" maze differing from all subsequent trials. Possibly, a prolonged trial familiarization could have attenuated this intercept. Prior to data collection, we decided against pseudo-randomization of maze complexity to not overwhelm participants with a challenging navigation task of complex mazes in our novel VR setup.

4.2 | Spatial specificity of posterior theta and alpha oscillations originating in or near retrosplenial complex

In order to assess whether theta and/or alpha activity express as a function of (allocentric) spatial location, we leveraged unique characteristics of mobile brain-body imaging (MoBI) to investigate multisensory integration via novel spectral maps. Because the output of the approach is a 2D map, we point out that tools for statistical inference readily exist in the field (see LIMO EEG, SPM, and others; Friston et al. 1994; Pernet et al. 2011). Again, we investigated changes as a result from repeated maze trials. We found that mapping ongoing spectral power in theta and alpha frequencies hinted at a potentially stronger (allocentric) spatial specificity of theta compared to alpha activity. Theta power increased in corners and dead ends in all mazes compared to the "full-map" baseline, see Figure 4b. Comparing the head location maps, Figure 3d, with the spectral maps in Figure 4b exhibits a similar pattern. Participants spent more time in corners and dead ends, at the same time power in theta and alpha was higher than baseline. Therefore, we contemplate that the spectral maps are likely strongly impacted by the processing around the touch events, both, in terms of motor planning and execution as well as visual processing and overall integration with respect to solving the spatial challenge at hand. Previously, Snider et al. (2013) described similar theta maps and found a correlation between (a) movement speed and theta synchronization and (b) theta synchronization and subsequent memory in a small-scale free exploration setting. In our case, theta synchronization was evident at the corners and dead ends, hinting at a possible pick up of medial temporal theta synchronicity in light of top-down, allocentric, prediction error signaling. A follow-up analysis, similar to Snider et al. (2013) implicating a role of subsequent (spatial) memory performance and theta synchronicity, correlating sketch map utility and the spatial theta maps, could provide further information on this theta signal but was beyond the scope of the current work.

In line with our findings of sketch maps not improving with repeated trials, we found that neither theta nor alpha maps changed with repeated trials, except in the "I" maze. In the "I" maze maps, a decrease in theta and alpha power from the initial to the later trials, see Figure 4b left, occurred at the dead end of the straight path. With the first "I" maze trial also differing significantly with respect to the exploration behavior, we hypothesize that participants were likely most strongly engaged in the task in this first trial (although going through a task familiarization period earlier). After solving the first trial, task engagement may have declined as indicated by sketch maps not improving and only efficiency improving, potentially indicating a saturation in "cognitive" signal-to-noise ratio.

4.3 | ERSP to wall touch do not change with repeated maze explorations

We hypothesized a shift from initial exploration to later knowledge exploitation behavior to impact event-related spectral activity in sources located in or near the retrosplenial complex. Grand average ERSP exhibited a significant early theta burst followed by alpha and beta desynchronization compared to the pre wall touch baseline (Figure 5). However, neither neural signature was significantly affected by repeated maze trials. For ERSP analyses, we selected a baseline immediately preceding, up until −100 ms, the visual wall touch feedback. Hence, baseline activity encompasses motor planning, preparation, and execution activity related to the hand reach, among others. Therefore, we conclude that the post-event activity more likely to be related to the processing of the visual stimulus and task-relevant components and *not* related to motor execution of the reach. While other sensorimotor clusters may uniquely reflect motor activity related to the hand movement, previous work targeting the same ROI observed similar activity patterns in spatial tasks without hand movements (Chiu et al., 2012; Gramann et al., 2010; Lin et al., 2015; Plank et al., 2010). Furthermore, single-trial analysis revealed a robust effect of the distance traveled between touches on the ERSP. Hence, ROIs located in deep posterior areas, such as the retrosplenial complex, unlikely reflect pure motor-driven modulation.

As we did not observe an effect of maze trials, however, signals related to spatial learning were not captured by the analysis of condition average ERSPs as was hypothesized, see Figure 5b. Other analytical approaches may prove fruitful to carve out EEG signals related to the formation of a cognitive map of an explored environment. Miyakoshi et al. (2020) conducted network analyses during spatial learning of a similar "audiomaze" task and report significant connectivity shifts between clusters of independent EEG sources localized to lingual gyrus and midcingulate cortex. Furthermore, we may have missed a transition effect from exploration to knowledge exploitation as allocentric hypotheses may likely be generated in deeper cortical structures, the medial temporal lobe (MTL). Because state-of-the-art EEG analyses are yet to find ways of capturing neural activity originating from deeper medial temporal sources, capturing signals of reflecting the consolidation of allocentric spatial relations may still prove challenging.

4.4 | Implicating posterior alpha in the formation and exploitation of mental spatial models

Evidence abounds for alpha oscillations in cortical information processing (Jensen & Mazaheri, 2010; Klimesch, 2012). Klimesch (2012) summarizes a role in both inhibition and timing processes of suppression and attentional selection. More specifically, parietal alpha oscillations along the dorsal processing stream have been implied in spatial direction of attention and spatial working memory tasks, see Freud et al. (2016) for a discussion. We observed alpha power to increase with distance traveled but to decrease with higher distances in case a wall different than the one previously encountered (Figure 6b). Recently, Deng et al. (2019) reported causal evidence for parietal alpha activity reflecting top-down attentional direction, but importantly so, only for spatial targets. In line with these findings, our results on alpha modulation by travel distance may reflect how attentional demands decrease (synchronization) with increasing travel distance along the same wall and hence may indicate how top-down attentional direction toward spatial targets may be directed from retrosplenial areas to the "parietal window" (Byrne et al., 2007).

We hypothesize that traveling along the same wall and repeatedly sampling it to maintain traveling orientation constituted confirmatory behavior. Further, increasing walking distance between touches potentially indicated a high-level of trust in the current heading direction. Therefore, alpha was not significantly impacted with regard to gating by inhibition across the dorsal processing stream (Jensen & Mazaheri, 2010). On the other hand, encountering new walls, potentially with unexpected orientations, provided novel evidence about the sampled structure, even more so after significant travel distance. We observed an alpha power decrease (desynchronization) with increasing travel distance when touching a new wall. Here, we suspect increased attentional demands, assuming prediction error to be maximal by means of the integration of self-movement cues in combination with the novel wall orientation. Subsequently, this current information constitutes maximally salient information in light of allocentric hypotheses testing. Therefore, facilitated message passing to "higher" allocentric hierarchies, possibly via attentional modulation, could be highly useful for future behavior.

Ultimately, our single-trial regression analysis revealed a theta increase for the main effect of encountering a wall differing from the previously touched. One can suspect that computations with regard to the heading direction may be reset upon confirmation of a new wall is picked up. However, our analysis did not distinguish between new walls following a turn around a corner or the change from one side of a path segment to touching the other side. In the latter case, allocentric heading does remain, whereas in the former case it changes by 90 degrees.

5 | CONCLUSION

When navigating invisible mazes, like finding your way in the dark, the peripersonal context is sampled by reaching and finding the nearest walls meanwhile building up a mental representation. Such mental representations can be leveraged to guide and optimize future behavior, such as taking less time to make your way to the next grocery store with a growling stomach. We confirmed such an optimization in participants' behavior, indicating the potential of the invisible maze task and similar paradigms to investigate event-related EEG signals during spatial learning. Targeting deep posterior EEG sources located in the retrosplenial complex, we did not observe a robust effect of discretized spatial learning in continuous EEG oscillations nor in event-related responses to wall touches, potentially in line with our findings that a highly accurate mental spatial representation manifested already after the initial maze exposure, or never at all. Through single-trial regression, we found that alpha activity was impacted by exploration behavior such as walking distance between subsequent spatial samples.

In summary, we showcase the capabilities of MoBI in VR, demonstrating several analysis approaches integrating motion capture and both continuous as well as event-related EEG signals in fully mobile, interacting, participants. Through single-trial regression, we conclude a role of alpha oscillations originating in deep posterior EEG sources located in the retrosplenial complex in multisensory action

and perception with a potential functional involvement in evidencing spatial predictions originating in medial temporal structures.

ACKNOWLEDGMENTS

We thank Jonna Jürs and Nora Moser for assisting with the data collection and John R. Iversen, Makoto Miyakoshi and Scott Makeig for fruitful discussions. This work was supported by the grant #01GQ1511 from the German Federal Ministry of Education and Research (BMBF; Bundesministerium für Bildung und Forschung).

CONFLICTS OF INTEREST

The author has no conflict of interest to declare.

AUTHOR CONTRIBUTION

L.G. and K.G. designed the research; L.G. collected the data, performed the data analysis, and wrote the first draft of the paper; K.G. and L.G. edited the paper.

Peer Review

The peer review history for this article is available at https://publons.com/publon/10.1111/ejn.15152.

DATA AVAILABILITY STATEMENT

Data relating to these experiments are available upon request from the corresponding author.

ORCID

Lukas Gehrke https://orcid.org/0000-0003-3661-1973
Klaus Gramann https://orcid.org/0000-0003-2673-1832

REFERENCES

Benjamini, Y., & Hochberg, Y. (1995). Controlling the false discovery rate: A practical and powerful approach to multiple testing. *Journal of the Royal Statistical Society: Series B (Methodological)*, *57*, 289–300.

Berger-Tal, O., Nathan, J., Meron, E., & Saltz, D. (2014). The exploration-exploitation dilemma: A multidisciplinary framework. *PLoS One*, *9*, e95693.

Bohbot, V. D., Copara, M. S., Gotman, J., & Ekstrom, A. D. (2017). Low-frequency theta oscillations in the human hippocampus during real-world and virtual navigation. *Nature Communications*, *8*, 14415.

Burgess, N. (2014). The 2014 Nobel Prize in physiology or medicine: A spatial model for cognitive neuroscience. *Neuron*, *84*(6):1120–1125.

Byrne, P., Becker, S., & Burgess, N. (2007). Remembering the past and imagining the future: A neural model of spatial memory and imagery. *Psychological Review*, *114*, 340–375.

Chiu, T. C., Gramann, K., Ko, L. W., Duann, J. R., Jung, T. P., & Lin, C. T. (2012). Alpha modulation in parietal and retrosplenial cortex correlates with navigation performance. *Psychophysiology*, *49*, 43–55.

Clark, A. (2013). Whatever next? Predictive brains, situated agents, and the future of cognitive science. *Behavioral and Brain Sciences*, *36*, 181–204.

Clark, B. J., Simmons, C. M., Berkowitz, L. E., & Wilber, A. A. (2018). The retrosplenial-parietal network and reference frame coordination for spatial navigation. *Behavioral Neuroscience*, *132*(5):416-429.

Cohen, J. (1960). A coefficient of agreement for nominal scales. *Educational and Psychological Measurement*, *20*, 37–46.

Delorme, A., & Makeig, S. (2004). EEGLAB: An open source toolbox for analysis of single-trial EEG dynamics including independent component analysis. *Journal of Neuroscience Methods*, *134*, 9–21.

Deng, Y., Reinhart, R. M., Choi, I., & Shinn-Cunningham, B. (2019). Causal links between parietal alpha activity and spatial auditory attention. *eLife*, *8*, 1–23. https://doi.org/10.7554/eLife.51184

Epstein, R. A. (2008). Parahippocampal and retrosplenial contributions to human spatial navigation. *Trends in Cognitive Sciences*, *12*(10), 388–396. https://doi.org/10.1016/j.tics.2008.07.004

Epstein, R. A., Patai, E. Z., Julian, J. B., & Spiers, H. J. (2017). The cognitive map in humans: Spatial navigation and beyond. *Nature Neuroscience*, *20*, 1504–1513. https://doi.org/10.1038/nn.4656

Freud, E., Plaut, D. C., & Behrmann, M. (2016). 'What' is happening in the dorsal visual pathway. *Trends in Cognitive Sciences*, *20*, 773–784. https://doi.org/10.1016/j.tics.2016.08.003

Friston, K. (2010). The free-energy principle: A unified brain theory? *Nature Reviews Neuroscience*, *11*, 127–138. https://doi.org/10.1038/nrn2787

Friston, K., FitzGerald, T., Rigoli, F., Schwartenbeck, P., O'Doherty, J., & Pezzulo, G. (2016). Active inference and learning. *Neuroscience and Biobehavioral Reviews*, *68*, 862–879. https://doi.org/10.1016/j.neubiorev.2016.06.022

Friston, K. J., Holmes, A. P., Worsley, K. J., Poline, J., Frith, C. D., & Frackowiak, R. S. (1994). Statistical parametric maps in functional imaging: A general linear approach. *Human Brain Mapping*, *2*, 189–210. https://doi.org/10.1002/hbm.460020402

Gamer, M., Lemon, J., Fellows, I., & Singh, P. (2010). Irr: various coefficients of interrater reliability.

Gehrke, L., Iversen, J. R., Makeig, S., & Gramann, K. (2018). The invisible maze task (IMT): Interactive exploration of sparse virtual environments to investigate action-driven formation of spatial representations. In S. Creem-Regehr, J. Schöning, & A. Klippel (Eds.), *Lecture notes in computer science (including subseries Lecture Notes in Artificial Intelligence and Lecture Notes in Bioinformatics)* (vol. 11034 LNAI, pp. 293–310). Springer International Publishing.

Goeke, C., Kornpetpanee, S., Köster, M., Fernández-Revelles, A. B., Gramann, K., & König, P. (2015). Cultural background shapes spatial reference frame proclivity. *Scientific Reports*, *5*, 11426. https://doi.org/10.1038/srep11426

Gramann, K. (2013). Embodiment of spatial reference frames and individual differences in reference frame proclivity. *Spatial Cognition and Computation*, *13*, 1–25. https://doi.org/10.1080/13875868.2011.589038

Gramann, K., Ferris, D. P., Gwin, J., & Makeig, S. (2014). Imaging natural cognition in action. *International Journal of Psychophysiology*, *91*, 22–29. https://doi.org/10.1016/j.ijpsycho.2013.09.003

Gramann, K., Gwin, J. T., Ferris, D. P., Oie, K., Jung, T. P., Lin, C. T., Liao, L. D., & Makeig, S. (2011). Cognition in action: Imaging brain/body dynamics in mobile humans. *Reviews in the Neurosciences*, *22*, 593–608. https://doi.org/10.1515/RNS.2011.047

Gramann, K., Hohlefeld, F. U., Gehrke, L., & Klug, M. (2018). Heading computation in the human retrosplenial complex during full-body rotation. *BioRxiv*, 417972.

Gramann, K., Müller, H. J., Eick, E.-M., & Schönebeck, B. (2005). Evidence of separable spatial representations in a virtual navigation

task. *Journal of Experimental Psychology: Human Perception and Performance*, *31*, 1199–1223. https://doi.org/10.1037/0096-1523.31.6.1199

Gramann, K., Onton, J., Riccobon, D., Mueller, H. J., Bardins, S., & Makeig, S. (2010). Human brain dynamics accompanying use of egocentric and allocentric reference frames during navigation. *Journal of Cognitive Neuroscience*, *22*(12), 2836–2849. https://doi.org/10.1162/jocn.2009.21369

Grieves, R. M., & Jeffery, K. J. (2017). The representation of space in the brain. *Behavioural Processes*, *135*, 113–131. https://doi.org/10.1016/j.beproc.2016.12.012

Hamburger, K., & Knauff, M. (2019). Odors can serve as landmarks in human wayfinding. *Cognitive Science*, *43*, e12798. https://doi.org/10.1111/cogs.12798

Hazen, N. L., Lockman, J. J., & Pick, H. L. (1978). The development of children's representations of large-scale environments. *Child Development*, *49*, 623. https://doi.org/10.2307/1128229

Hegarty, M., Richardson, A. E., Montello, D. R., Lovelace, K., & Subbiah, I. (2002). Development of a self-report measure of environ- mental spatial ability. *Intelligence*, *30*, 425–447.

Hohwy, J. (2016). The self-evidencing brain. *Nous*, *50*, 259–285.

Huk, A. C., & Shadlen, M. N. (2005). Neural activity in macaque parietal cortex reflects temporal integration of visual motion signals during perceptual decision making. *Journal of Neuroscience*, *25*, 10420–10436.

Ishikawa, T., & Montello, D. R. (2006). Spatial knowledge acquisition from direct experience in the environment: Individual differences in the development of metric knowledge and the integration of separately learned places. *Cognitive Psychology*, *52*, 93–129.

Ito, H. T., Zhang, S. J., Witter, M. P., Moser, E. I., & Moser, M. B. (2015). A prefrontal-thalamo-hippocampal circuit for goal-directed spatial navigation. *Nature*, *522*, 50–55.

Jensen, L., Piaget, J., Inhelder, B., Langdon, F. J., & Lunzer, J. L. (1958). The child's conception of space. Art Education.

Jensen, O., & Mazaheri, A. (2010). Shaping functional architecture by oscillatory alpha activity: Gating by inhibition. *Frontiers in Human Neuroscience*, *4*, 186.

Jungnickel, E., Gehrke, L., Klug, M., & Gramann, K. (2019). MoBI-mobile brain/body imaging. In H. Ayaz & F. Dehais (Eds.), *Neuroergonomics: The brain at work and in everyday life* (pp. 59–63). Academic Press.

Kennedy, R. S., Lane, N. E., Berbaum, K. S., & Lilienthal, M. G. (1993). Simulator sickness questionnaire: An enhanced method for quantifying simulator sickness. *The International Journal of Aviation Psychology*, *3*, 203–220.

Klimesch, W. (2012). Alpha oscillations, attention, and controlled access to stored information. *Trends in Cognitive Sciences*, *16*, 606–617.

Kozhevnikov, M., & Hegarty, M. (2001). A dissociation between object manipulation spatial ability and spatial orientation ability. *Memory and Cognition*, *29*, 745–756.

Kravitz, D. J., Saleem, K. S., Baker, C. I., & Mishkin, M. (2011). A new neural framework for visuospatial processing. *Nature Reviews Neuroscience*, *12*, 217–230. https://doi.org/10.1038/nrn3008

Kriegeskorte, N., Simmons, W. K., Bellgowan, P. S., & Baker, C. I. (2010). Circular inference in neuroscience: The dangers of double dipping. *Journal of Vision*, *8*(6), 88. https://doi.org/10.1167/8.6.88

Kuznetsova, A., Brockhoff, P. B., & Christensen, R. H. B. (2017). lmerTest package: Tests in linear mixed effects models. *Journal of Statistical Software*, *82*, 1–26.

Lenth, R., Singmann, H., Love, J., Buerkner, P., & Herve, M. (2020). Package 'emmeans'. R package version 1.4.6, 34, 216–221.

Liang, M., Starrett, M. J., & Ekstrom, A. D. (2018). Dissociation of frontal-midline delta-theta and posterior alpha oscillations: A mobile EEG study. *Psychophysiology*, *55*(9), e13090. http://dx.doi.org/10.1111/psyp.13090

Lin, C. T., Chiu, T. C., & Gramann, K. (2015). EEG correlates of spatial orientation in the human retrosplenial complex. *NeuroImage*, *120*, 123–132. https://doi.org/10.1016/j.neuroimage.2015.07.009

Loomis, J. M., Klatzky, R. L., Golledge, R. G., Cicinelli, J. G., Pellegrino, J. W., & Fry, P. A. (1993). Nonvisual navigation by blind and sighted: Assessment of path integration ability. *Journal of Experimental Psychology: General*, *122*, 73–91. https://doi.org/10.1037/0096-3445.122.1.73

Madl, T., Chen, K., Montaldi, D., & Trappl, R. (2015). Computational cognitive models of spatial memory in navigation space: A review. *Neural Networks*, *65*, 18–43. https://doi.org/10.1016/j.neunet.2015.01.002

Makeig, S., Gramann, K., Jung, T. P., Sejnowski, T. J., & Poizner, H. (2009). Linking brain, mind and behavior. *International Journal of Psychophysiology*, *73*, 95–100. https://doi.org/10.1016/j.ijpsycho.2008.11.008

Mitchell, A. S., Czajkowski, R., Zhang, N., Jeffery, K., & Nelson, A. J. D. (2018). Retrosplenial cortex and its role in spatial cognition. *Brain and Neuroscience Advances*, *2*, 239821281875709. https://doi.org/10.1177/2398212818757098

Miyakoshi, M., Gehrke, L., Gramann, K., Makeig, S., & Iversen, J. R. (2020). The Audiomaze: An EEG and motion capture study of human spatial navigation in sparse augmented reality. *European Journal of Neuroscience*, *00*, 1–10.

Moser, E. I., Kropff, E., & Moser, M.-B. (2008). Place cells, grid cells, and the brain's spatial representation system. *Annual Review of Neuroscience*, *31*, 69–89. https://doi.org/10.1146/annurev.neuro.31.061307.090723

Ojeda, A., Bigdely-Shamlo, N., & Makeig, S. (2014). MoBILAB: An open source toolbox for analysis and visualization of mobile brain/body imaging data. *Frontiers in Human Neuroscience*, *8*, 1–9. https://doi.org/10.3389/fnhum.2014.00121

O'keefe, J., & Nadel, L. (1979). The hippocampus as a cognitive map. *Behavioral and Brain Sciences*, *2*, 487–494.

Oostenveld, R., & Oostendorp, T. F. (2002). Validating the boundary element method for forward and inverse EEG computations in the presence of a hole in the skull. *Human Brain Mapping*, *17*(3), 179–192. https://doi.org/10.1002/hbm.10061

Palmer, J., Kreutz-Delgado, K., & Makeig, S. (2011). AMICA: An adaptive mixture of independent component analyzers with shared components. Technical report. Swartz Center for Computational Neuroscience, 1–15.

Pernet, C. R., Chauveau, N., Gaspar, C., & Rousselet, G. A. (2011). (2011) LIMO EEG: A toolbox for hierarchical linear modeling of electroencephalographic data. *Computational Intelligence and Neuroscience*, *2011*, 1–11. https://doi.org/10.1155/2011/831409

Pernet, C. R., Latinus, M., Nichols, T. E., & Rousselet, G. A. (2015). Cluster-based computational methods for mass univariate analyses of event-related brain potentials/fields: A simulation study. *Journal of Neuroscience Methods*, *250*, 85–93. https://doi.org/10.1016/j.jneumeth.2014.08.003

Pion-Tonachini, L., Kreutz-Delgado, K., & Makeig, S. (2019). ICLabel: An automated electroencephalographic independent component

classifier, dataset, and website. *NeuroImage*, *198*, 181–197. https://doi.org/10.1016/j.neuroimage.2019.05.026

Plank, M., Müller, H. J., Onton, J., Makeig, S., & Gramann, K. (2010). Human EEG correlates of spatial navigation within egocentric and allocentric reference frames. Lecture Notes in Computer Science (including subseries Lecture Notes in Artificial Intelligence and Lecture Notes in Bioinformatics), 6222 LNAI, 191–206.

RStudio Team (2019). RStudio: Integrated Development for R. *RStudio*. Boston, MA: PBC. http://www.rstudio.com/

Schinazi, V. R., Nardi, D., Newcombe, N. S., Shipley, T. F., & Epstein, R. A. (2013). Hippocampal size predicts rapid learning of a cognitive map in humans. *Hippocampus*, *23*, 515–528. https://doi.org/10.1002/hipo.22111

Siegel, A. W., & White, S. H. (1975). The development of spatial representations of large-scale environments. *Advances in Child Development and Behavior*, *10*, 9–55.

Snider, J., Plank, M., Lynch, G., Halgren, E., & Poizner, H. (2013). Human cortical θ during free exploration encodes space and predicts subsequent memory. *Journal of Neuroscience*, *33*, 15056–15068.

Stachenfeld, K. L., Botvinick, M. M., & Gershman, S. J. (2017). The hippocampus as a predictive map. *Nature Neuroscience*, *20*, 1643–1653. https://doi.org/10.1038/nn.4650

Starrett, M. J., & Ekstrom, A. D. (2018). Perspective: Assessing the flexible acquisition, integration, and deployment of human spatial representations and information. *Frontiers in Human Neuroscience*, *12*, 1–9. https://doi.org/10.3389/fnhum.2018.00281

Tolman, E. C. (1948). Cognitive maps in rats and men. *Psychological Review*, *55*, 189–208. https://doi.org/10.1037/h0061626

Vann, S. D., Aggleton, J. P., & Maguire, E. A. (2009). What does the retrosplenial cortex do? *Nature Reviews Neuroscience*, *10*, 792–802. https://doi.org/10.1038/nrn2733

Weisberg, S. M., & Newcombe, N. S. (2018). Cognitive maps: Some people make them, some people struggle. *Current Directions in Psychological Science*, *27*, 220–226. https://doi.org/10.1177/0963721417744521

Whitlock, J. R., Sutherland, R. J., Witter, M. P., Moser, M. B., & Moser, E. I. (2008). Navigating from hippocampus to parietal cortex. *Proceedings of the National Academy of Sciences of the United States of America*, *105*, 14755–14762. https://doi.org/10.1073/pnas.0804216105

Yang, F. C., Jacobson, T. K., & Burwell, R. D. (2017). Single neuron activity and theta modulation in the posterior parietal cortex in a visuospatial attention task. *Hippocampus*, *27*(3), 263–273. https://doi.org/10.1002/hipo.22691

How to cite this article: Gehrke L, Gramann K. Single-trial regression of spatial exploration behavior indicates posterior EEG alpha modulation to reflect egocentric coding. *Eur J Neurosci*. 2021;54:8318–8335. https://doi.org/10.1111/ejn.15152